Defense Technical Information Center
Compilation Part Notice

ADP013672

TITLE: Direct Numerical Simulation of Turbulent Flow and Heat Transfer in a Square Duct at Low Reynolds Number

DISTRIBUTION: Approved for public release, distribution unlimited

This paper is part of the following report:

TITLE: DNS/LES Progress and Challenges. Proceedings of the Third AFOSR International Conference on DNS/LES

To order the complete compilation report, use: ADA412801

The component part is provided here to allow users access to individually authored sections of proceedings, annals, symposia, etc. However, the component should be considered within the context of the overall compilation report and not as a stand-alone technical report.

The following component part numbers comprise the compilation report:
ADP013620 thru ADP013707

DIRECT NUMERICAL SIMULATION OF TURBULENT FLOW AND HEAT TRANSFER IN A SQUARE DUCT AT LOW REYNOLDS NUMBER

M. PILLER AND E. NOBILE

Dipartimento di Ingegneria Navale, del Mare e per l'Ambiente
Sezione di Fisica Tecnica
University of Trieste, 34127 Trieste – ITALY

Abstract. In this paper, we present the results from Direct Numerical Simulations of turbulent, incompressible flow through a square duct, with an imposed temperature difference between two opposite walls, while the other two walls are assumed perfectly insulated. The mean flow is sustained by an imposed, mean pressure gradient. The most interesting feature, characterizing this geometry, consists in the presence of turbulence-sustained mean secondary motions in the cross-flow plane.

In this study, we focus on weak turbulence, in that the Reynolds number, based on bulk velocity and hydraulic diameter, is about 4450. Our results indicate that secondary motions do not affect dramatically the global parameters, like friction factor and Nusselt number, in comparison with the plane-channel flow. This issue is investigated by looking at the distribution of the various contributions to the total heat flux, with particular attention to the mean convective term, which does not appear in the plane channel flow.

1. INTRODUCTION

In this work, we adopt Direct Numerical Simulation (DNS hereafter) as a convenient tool for studying both the velocity and temperature fields in the presence of solid corners. A square duct is a suitable geometry, in this respect, due to its high degree of symmetry. An imposed pressure drop drives the flow, while the temperature field is generated by the two horizontal walls, kept at constant, different temperatures $\pm T_w$. The vertical walls are assumed perfectly insulated. The Reynolds number, based on hydraulic diameter and bulk velocity, is approximately 4450, while the Prandtl number

is assumed 0.71, representative of air. The Reynolds number Re_τ, based on hydraulic diameter and friction velocity, is 300, as in [1].

From the present simulations, the maximum secondary mean velocity was found to be about 2% of the centerline streamwise velocity. The results clearly indicate that, even though both the heat transfer rate and friction factor are not strongly affected by the presence of mean secondary motions, their effect on the distribution of various quantities within the flow field can not be neglected. For instance, we report the distributions of both the shear stress and the heat flux, at the horizontal walls. Interesting features, clearly connected with the presence of mean secondary motions, characterize these quantities.

2. PROBLEM DEFINITION AND SCALES

The full, time-dependent incompressible Navier Stokes and energy equations are solved directly, without any modelling assumption regarding the turbulent velocity and temperature fields. Simplifying assumptions are made, in that viscous energy dissipation and buoyancy forces are neglected, and the fluid properties are assumed constant. The hydraulic diameter, $D_h = 2h$, the friction velocity, $u_\tau = (-\Delta P\,D_h/4\rho\,\lambda_x)^{1/2}$, and the wall-temperature T_w are used in order to define dimensionless quantities. Domain dimensions are indicated in figure 1, which shows a sketch of the duct. Two simulations have been considered, and they differ in the streamwise domain length, λ_x, which was $4\pi h$ for Case A, and $12\pi h$ for case B. Grids with $200 \times 127 \times 127$ and $600 \times 127 \times 127$ computational cells were used in simulations A and B, respectively, so that the resolution was identical in both cases. The grid spacing was $\Delta x^+ = 9.42$, $\Delta y^+ = \Delta z^+ = 0.45 \div 4.6$. This resolution was judged to be adecquate in [1].

We adopted a second-order, Finite-Volume algorithm in order to solve the flow and energy equations [2]. Decoupling of the continuity from the momentum equations is performed by a classical second-order projection scheme [4]. The computational grid is uniform in the homogeneous, streamwise direction, while an hyperbolic-tangent distribution is adopted in both cross-stream directions.

All data reported here originate from case B. Statistics were acquired over 2 Large Eddy Turnover Times (LETOTS). By using the bulk-velocity reported in table 1, this time interval corresponds to about 1.6 flow-through times.

TABLE 1. Global statistics for Case B, compared with results for the channel flow, and with a DNS for a square duct.

	Case B	Channel [6]	Ref. [1]
Re_b	4453	4560	4410
U_b	14.84	15.2	14.7
f	0.0363	0.035	0.037
Nu	4.89	5.08	

3. RESULTS AND DISCUSSION

Mean secondary motions, shown in figure 2(a), result in four couples of counter-rotating corner-vortices, which carry high-momentum fluid from the core-region toward the corners, and low-momentum fluid away from the walls. The effect of the mean secondary motions on the streamwise velocity distribution is evident, in that isotach lines are bent toward the corners. Weaker vortices, located on both sides of the wall bisectors, were reported in [1], but have not been observed from the mean data of the present simulations. A conditional sampling of the flow field showed the presence of these vortices (figure 2b); the flow field was acquired only when the value of the streamwise vorticity, averaged in the marked box, was smaller than -3.0, in wall units. Since these vortices are highly intermittent, a longer averaging time would be required to capture them in the mean data. At higher Reynolds numbers these vortices have not been observed [3], and therefore they could be a low-Reynolds feature.

Mean temperature profiles at various distances from the left wall are presented in figure 3. The temperature distribution on a wall-bisector compares well with that of the channel flow, at the same Re_τ [6]. The temperature profile at $y^+ = 35$ from the left wall is clearly influenced by the corner vortices, resulting in a more distorted profile than at the wall-bisector. The bending of the temperature profile at $y^+ = 3.3$ indicates the presence of significant turbulent activity at this location. This is quite surprising, since we are well within the viscous sublayer. However, the side-walls are assumed perfectly insulated, thus allowing the temperature fluctuations to extend down to the wall, as can be verified in figure 4(a). Moreover, the w' fluctuations assume large values in the close proximity of the vertical walls, before vanishing at the wall (figure 4b). Thus, the turbulent mixing affects the mean temperature distribution, even in the viscous sublayer on the vertical walls.

Values of the bulk-Reynolds number, Re_b, the mean Nusselt number, Nu and the friction factor, f, are reported in table 1. The friction factor

agrees, to better than 1%, with empirical correlations available for this geometry [5], when the laminar equivalent diameter, $D_l = \left(1 + \sqrt{2}\right) h$, is used. The Nusselt number is defined as $Nu = (q_w\, 2h) / [k\, (\Delta\, T_w)]$, and can be evaluated from the DNS data as

$$Nu = \frac{1}{2} \left\langle \int_{-1/2}^{+1/2} Re_\tau\, Pr\, \overline{w\vartheta} - \frac{\partial T}{\partial z} dy \right\rangle$$

where the brackets indicate avaraging along z, and all quantities are dimensionless. The Nusselt number from present simulations is only 3.8% smaller than the Nusselt number evaluated for the channel flow [6].

A possible interpretation of this fact could be that the decrease of turbulent heat transfer ,near the vertical walls, is partially compensated by the mean convective heat flux in the core region. This picture is confirmed by figure 5, which shows the total, the turbulent and the mean convective heat-flux distributions. The gray sfumature corresponds to values from -11.9 (black) to 11.9 (white). The total heat flux ranges from -3.09 to 11.90. The turbulent heat flux assues values between -4.5×10^{-5} and 6.24. For comparison, the turbulent heat flux in the channel flow [6] assumes an almost constant value of 6.4 in the core region, when scaled by the friction velocity and the temperature difference between the walls. The mean convective heat-flux is comprised between -6.05 and 9.95. The mean convective heat-flux is defined as follows:

$$q''_{conv} = 1/2\, Re_\tau\, Pr\, (W/u_\tau)\, (T/T_w)$$

Figure 5 suggests that there is a *corridor* through which the heat flows from the bottom toward the top wall. Several *obstacles* tend to reduce this flow. First, the turbulent heat-flux is reduced near the vertical walls, due to the presence of the velocity boundary layer. Second, the corner vortices create mean convective heat fluxes, WT, which *pump* heat in the positive z direction near the horizontal walls bisector, but they also create a negative, mean convective heat flux, near the vertical walls. This effect can be recognized in figure 5(c), where regions of negative mean convective heat-flux appear in correspondence of the corner vortices.

Figures 6 and 7 show the distributions of the mean, total shear stress and heat flux at the bottom wall, respectively. The shear stress vanishes at the vertical walls, due to the presence of stagnation regions at the corners. Three local maxima are evident in the shear-stress profile at the wall. The near-wall peaks are located in the region below the corner-vortices, and are clearly generated by the intense impingement of high-speed fluid, carried from the vortex, against the wall. The local minima are located where the corner vortices carry low-speed fluid away from the wall, toward the core

region. The central peak in the wall shear stress is known to be a low-Reynolds number effect [1]. Clustering and widening of streamwise velocity contours, evident in figure 2, allow an immediate interpretation of the shear-stress behavior. The local heat flux, figure 7, shows a behavior similar to the shear stress. In this case, however, the central maximum is smaller than the side ones. The lateral peaks in the wall heat flux profile are located below regions of high mean convective heat flux, which is advected by the corner vortices and carried toward the bisector of the horizontal wall. This can be appreciated in figure 5(c).

The $\overline{w'\theta'}$ turbulent heat flux decreases near the vertical walls, due to the combined effect of a reduction in the intensity of both w' and θ', as shown in figure 4. Moreover, there is also a loss of correlation between w' and θ', in regions close to the vertical walls, as reported in figure 8, which shows the distribution of $\overline{w'\theta'}/w'\theta'$. In figure 8 black corresponds to 0 and white corresponds to 1. The correlation coefficient is particularly low in correspondence of the corner vortices attached to the vertical walls ($y/2h \approx 0.4$, $z/2h \approx 0.35$). Just below this area there is a region of high correlation coefficient, attached to the horizontal wall. It corresponds to the high heat flux region evidenced in figures 5(a),(c). The loss of correlation of w' and ϑ' close to the vertical walls is an expected feature, considering the different boundary conditions imposed on velocity and temperature.

Streamwise power spectra for both the temperature and the streamwise velocity fluctuations are shown in figure 9. They are normalized in such a way that the area under each curve equals unity. At the centerline the spectral distributions of temperature and velocity fluctuations are very close to each other, in the whole wavenumber range. In the corner region there is still substantial agreement between ϑ' and u' spectra, although the second tend to decay slightly faster. As one might expect, in the corner region both viscosity and molecular conductivity are more effective in damping velocity and temperature fluctuations, and both spectra decay faster than at the centerline, at least in the intermediate range of wavenumbers. At very large wavenumbers the spectra evaluated at both locations collapse on each other; this is quite surprising, since the characteristics of both the velocity and temperature fields are fairly different, in these regions. Aliasing effects show up just in a very-high wavenumber range, which accounts for negligible energy content. This shows that the adopted streamwise resolution was adequate, in order to represent the main features of both the flow and temperature fields.

4. CONCLUDING REMARKS

In this work we presented results obtained from DNS of turbulent forced convection in a square duct. In particular, DNS data for the temperature field were not available before, to the best of our knowledge.

Streamwise power spectra for both streamwise velocity and temperature fluctuations were calculated, at various cross-stream locations. Some peculiar aspects regarding the decay of the highest wave-number components were pointed out.

The influence of mean secondary motions on both the temperature and velocity fields was discussed. The maximum intensity of these motions was found to be about 2% of the maximum mean streamwise velocity. The comparison of the duct flow with the plane-channel flow led to the observation that global parameters, like the Fanning friction-factor and the Nusselt number, are not strongly affected by the presence of the side-walls, while the distribution of the local shear-stress and heat-flux at a wall shows characteristic patterns, whose origin appears to be related to the mean secondary motions.

The present work constitute a base for future investigations, regarding unstably stratified internal flows. We are currently running other simulations for the square-duct flow, in order to investigate the combined influence of mean secondary motions and buoyancy forces, on both the velocity and temperature fields.

References

1. Gavrilakis, S. (1992) Numerical simulation of low-Reynolds-number turbulent flow through a straight square duct *J. Fluid Mech.*, **Vol. no. 244**, pp. 104–129.
2. Onesti, L. (1995) *High Performance Parallel Computing on the Cray T3D – CFD Applications*, Batchelor Thesis (*in Italian*), University of Trieste, Italy.
3. Gessner, F.B. and Jones, J.B. (1965) On some aspects of fully-developed turbulent flow in rectangular channels *J. Fluid Mech.*, **Vol. no. 23**, pp. 689–713.
4. Gresho, P.M. (1990) On the theory of semi-implicit projection method for viscous incompressible flow and its implementation via a finite element method that also introduces a nearly consistent mass matrix. Part 1: theory. *Int. J. Numer. Methods Fluids*, **Vol. no. 11**, pp. 587–620.
5. Kakac, S., Shah, R.K. and Aung, W. (1987) *Handbook of Single-Phase Convective Heat Transfer*, Chapter 4, John Wiley and Sons.
6. Iida, O. and Kasagi, N. (2001). Heat transfer of fully developed turbulent channel flowwith iso-thermal walls. *Online database: www.thtlab.t.u-tokyo.ac.jp, case # CH122_PG.WL4*
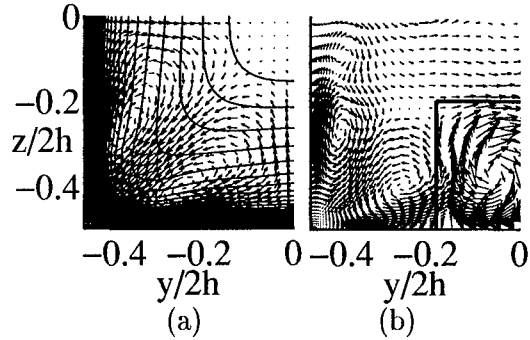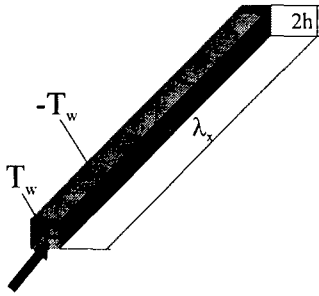
Figure 1. Sketch of the computational domain.

Figure 2. (a) Mean secondary motions and Mean streamwise velocity contours on a cross-stream plane. (b) Conditional sampling of the secondary motions.
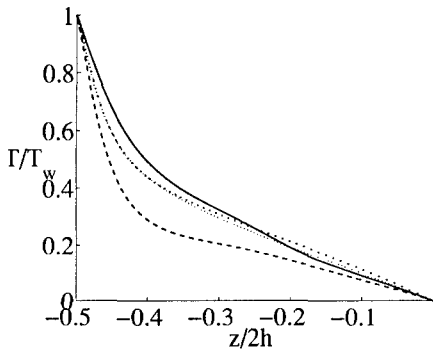

Figure 3. Mean temperature profiles at several distances y_w^+ from a vertical wall. ——: $y_w^+ = 3.3$; – – –: $y_w^+ = 35$; — · —: $y_w^+ = 150$. Data for the plane channel flow [6] are shown as symbols.
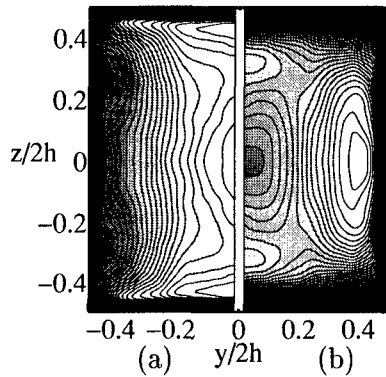

Figure 4. ϑ' (left) and w' (right) fluctuations, scaled by their maximum values. From black to white: 0.0 to 1.0.
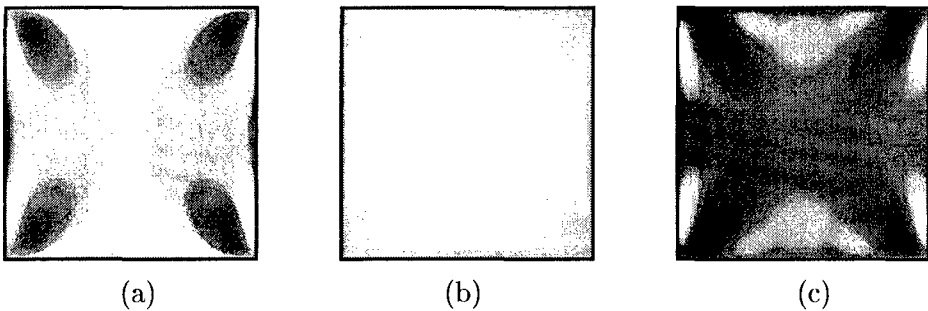
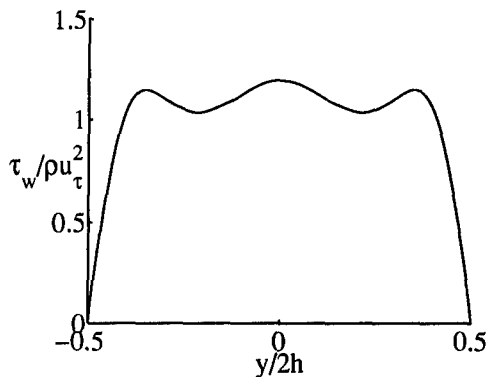*Figure 5.* Heat-flux in the z direction. (a): total; (b) turbulent; (c) convective.

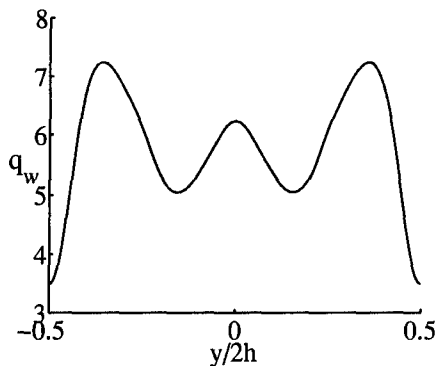*Figure 6.*   Wall shear-stress.

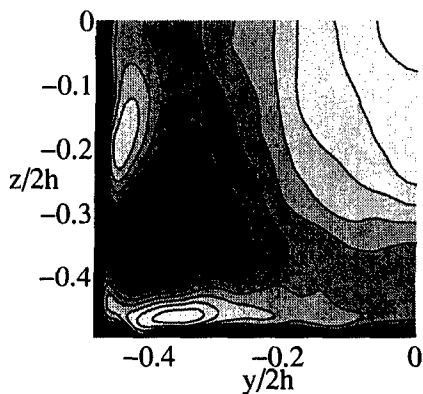*Figure 7.*   Wall heat-flux.

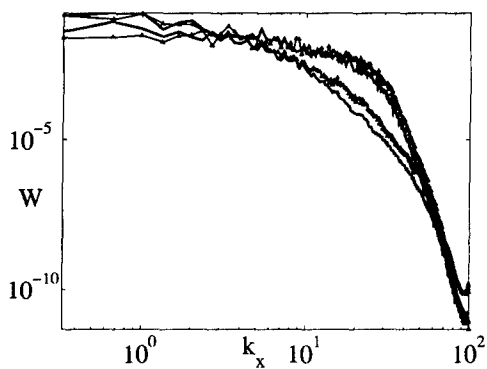*Figure 8.* $\overline{v'\vartheta'}/v'\vartheta'$ contours on a cross-flow plane.

Figure 9.   Spectra of streamwise velocity and temperature fluctuations, at the center-line (upper curves) and at $y^+ = z^+ = 15$ (lower curves). Thick solid curves: spectra of streamwise velocity fluctuations. Tiny curves with symbols: spectra of temperature fluctuations.